J. Phys. Chem. A **2004,** *108,* 9453−9460

Time-Dependent Density Functional Theory Investigation of Electronic Excited States of Tetraoxaporphyrin Dication and Porphycene

Jian Wan,*,† Yanliang Ren,† Jianming Wu,‡ and Xin Xu*,‡

Key Laboratory of Pesticide & Chemical Biology, College of Chemistry, Central China Normal University, Wuhan 430079, China, and State Key Laboratory for Physical Chemistry of Solid Surfaces, Department of Chemistry, Center for Theoretical Chemistry, Xiamen University, Xiamen 361005, China

Received: June 25, 2004; In Final Form: August 13, 2004

The electronic ground state and the singlet vertical excited states of tetraoxaporphyrin dication (TOPDC) and porphycene have been investigated by using time-dependent density functional theory (TDDFT) for the first time. The solvation effects on the excitation energies for TOPDC in 96% H_2SO_4 and porphycene in 2-methyltetrahydrofuran are taken into account by using the polarized continuum model (PCM). The TDDFT-PCM computed results show an obvious red shift of the excitation energies of the B (Soret) bands, leading to a much better agreement with the UV/vis absorption spectra in solutions than the previous semiempirical calculations in vacuo.

I. Introduction

The chemistry of porphyrinoids (porphyrin structural variants) has developed with breathtaking speed over the past decade. Recent progress in synthetic chemistry[1,2] has led to the appearance of a large number of new porphyrinoids with changes of structures, sizes, and heteroatoms.[3−5] Some of the recent important representatives are, for example, the O-, S-, and Se-analogues of porphyrins,[6] the inverted porphyrins,[7,8] the contracted porphyrins,[9] and the N-confused porphyrins.[10,11]

It is not surprising that such huge porphyrinoid families have been synthesized because typical electron donors in natural photosynthetic reaction centers are free base and metalated porphyrine systems. In addition to their possible application to anticancer drugs in photodynamic therapy,[12] their unique photochemical properties make them potential candidates for luminescent materials. For example, the diacids of sulfonatophenyl-substituted porphyrins were found recently to form aggregates in proper conditions, accompanying dramatic changes in UV/vis absorption and luminescence spectra.[13−18] These porphyrin aggregates have regular high-order structures and show close resemblance in structures and photochemical properties with the chlorophyll aggregates in natural light-harvesting systems.

The theoretical study of the electronic excitations of porphyrinoids can provide a sophisticated understanding and the assignments of UV/vis absorption and luminescence spectra of porphyrinoids. The gas-phase electronic absorption spectrum of free base porphyrin has been the subject of many theoretical studies.[19−22] On the other hand, the O-, S-, and Se-analogues of porphyrins and other types of porphyrinoids have received little theoretical attention.[23,24]

In this study, we present the first time-dependent density functional theory (TDDFT)[25−28] investigation of the singlet vertical excited states of tetraoxaporphyrin dication (TOPDC) and porphycene. These are selected as examples to represent two different subgroups within the new porphyrinoids. To compare with the experimental UV/vis absorption spectra for TOPDC in 96% H_2SO_4[4,5] and porphycene in 2-methyltetrahydrofuran (2-MTHF) solutions,[4] the solvation effects on the excitation energies are investigated by combining the TDDFT with the polarized continuum model (PCM[28−30]) method. The present TDDFT-PCM calculation results show a red shift of excitation energy for the B (Soret) band for both TOPDC and porphycene upon solvation, in good agreement with the experimental data.

In section II, we outline the computational details. Calculation results and discussions are presented in section III. A summary is given in section IV.

II. Computational Details

All quantum mechanical calculations were carried out using the B3LYP flavor of density functional theory (DFT),[31] which includes Becke's nonlocal gradient corrections[32] to the Slater local exchange functional[33] and some exact Hartree−Fock (HF) exchange, as well as the Vosko−Wilk−Nusair local correlation functional[34] and the Lee−Yang−Parr correlation functional.[35]

The polarizable solvation model (PCM) was employed to describe the effect of solvent,[28−30] whose reliability for both ground and excited states is well documented. In this approximation, the solvent is represented as a structureless infinite continuum, characterized by its macroscopic dielectric constant (ϵ), numeral density (ρ), and so forth. The cavity for the solute is built as the envelopes of spheres centered on the solute atoms or atomic group, and then a sphere of radius (R_{solv}) of the solvent is rolled over this surface to obtain a smooth surface. At each self-consistent field (SCF) step, we calculate the reaction field generated by the solvent due to the electrostatic field of the solute wave function. This reaction field is then included in the Fock operator (Kohn−Sham Hamiltonian) to calculate the orbitals of the DFT wave function of the solute. This process is continued until self-consistent. When time-dependent DFT is used to study the vertical electronic excitation processes, which have a characteristic time smaller than the solvent relaxation time, a delay is observed in the solvent response such that nonequilibrium solvation in terms of a "fast" dielectric

---

* To whom correspondence should be addressed. E-mail: jianwan@mail.ccnu.edu.cn; xinxu@xmu.edu.cn.

† Central China Normal University.

‡ Xiamen University.

10.1021/jp047219a CCC: $27.50

constant (ϵ_f) has to be used.[28] For the TOPDC system, we use $\epsilon = 100.0$, $\epsilon_f = 2.009$, $\rho = 0.01124$ Å^{-3}, and $R_{solv} = 2.198$ Å to describe the concentrated sulfuric acid solvent; while for the porphycene solution, we use $\epsilon = 6.97$, $\epsilon_f = 1.978$, $\rho = 0.006013$ Å^{-3}, and $R_{solv} = 2.71$ Å to represent the 2-MTHF solvent. These numbers are derived from the related experimental data.[36] Experiments showed that there is no excitation transfer from solute to solvent for both TOPDC and porphycene systems, which justifies the employment of the PCM.[4,5]

Geometry optimizations were performed with the 6-31G(d)[37] basis set both in vacuo and in solution. For each gas-phase geometry, vibrational frequencies are calculated analytically to ensure it to be a true local minimum (containing only positive frequencies). To investigate the possible counterion effect in the TOPDC system, two ClO_4^- or two HSO_4^- were explicitly included and the full geometry optimization was performed on the perchlorate TOPDC or the hydrogen sulfate TOPDC. The optimized geometry parameters were compared with those from the bare TOPDC ion and those from the X-ray structure analysis.[4,23]

TDDFT calculations were carried out at the optimized structures both in vacuo and in solution. In the TDDFT calculations, Dunning's augmented correlation consistent basis set aug-cc-pVDZ[38] was used for all non-hydrogen atoms (one augmented *d*-type diffuse function was removed for all the calculations), and cc-pVDZ[39] was used for all H atoms. To investigate the basis set effects, comparison was also performed at the TDDFT(B3LYP)/6-31G(d) and TDDFT(B3LYP)/6-311G(d) levels for the excited states of TOPDC in the gas phase.

All calculations were performed using the Gaussian 03 program suite[40] on a SGI/Origin-300 server.

III. Results and Discussion

A. Ground-State Properties. There has been a long-lasting interest in the theoretical prediction of the geometric and the electronic structures of porphyrinoids.[41−46] Following Gouterman's pioneering work,[41] the porphyrinoid's structures have been frequently interpreted as an internal [18]annulene-like conjugation path embedded in the macrocycles.[43] Later, Michl and co-workers argued that an even better model is provided by a [20]annulene-dication conjugation path.[43] We depict both [18]- and [20]annulene structures for TOPDC in Figure 1. It was concluded that the electronic structures of porphyrinoids are ruled by the competition between local cyclic interactions in the subunits and the delocalization over the whole macrocycle.[43] The electron correlation effects were found to play an important role to stabilize the delocalized structure with high symmetry.[4,23]

The key data from the X-ray structure analysis on perchlorate TOPDC crystal are summarized in Table 1. Along with the NMR results and IR results, it was concluded that TOPDC adopts a D_{4h} symmetry.[4,23] These results may be interpreted as lending support to the [20]annulene-dication model, as such C−C bond lengths for type 1 and type 9 are the same. We performed the geometry optimizations with no symmetry constraint at the B3LYP/6-31G(d) level. The key parameters of the optimized ground-state geometry of TOPDC are presented in Table 1. As can be seen from the data in Table 1, the optimized geometry practically converges to a D_{4h} symmetry, in agreement with the experimental findings.[4,23] Typically the optimized C−C bond length is slightly longer ($\leq$0.03 Å) than the corresponding bond length of the X-ray structures.[4] The maximum elongation is observed at the type 1 C−C bond. We find that B3LYP may exaggerate the delocalization effect. Hence the deviation between type 1 and type 2 C−C bonds is only 0.045 Å in the optimized TOPDC structure, while it is 0.065 Å in the X-ray structure.[4]

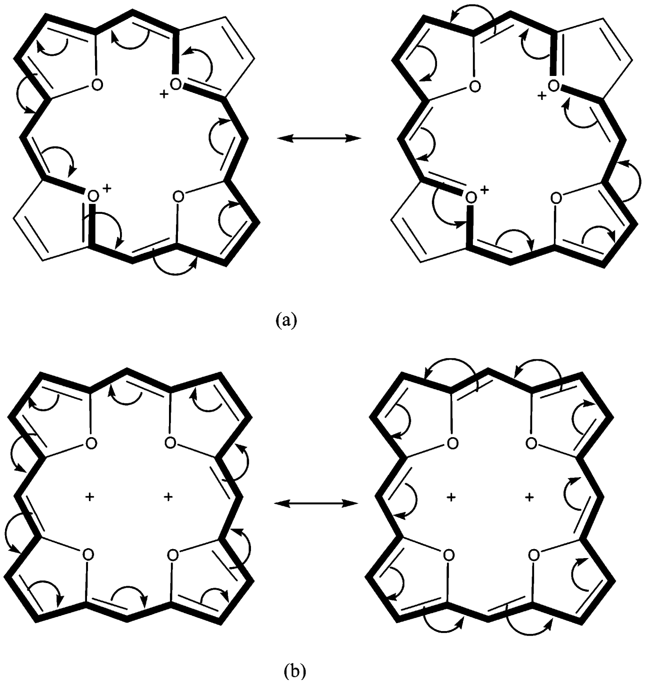

Figure 1. (a) [18]- and (b) [20]annulene structures for TOPDC.

TABLE 1: Experimental and Optimized Bond Lengths (Å) for TOPDC under D_{4h} Symmetry

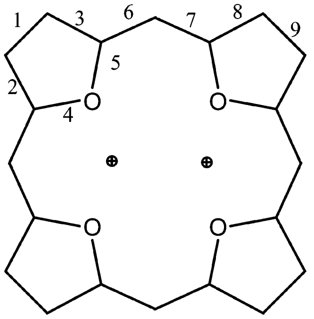

bond	X-ray (refs 4 and 23)	B3LYP/ 6-31G(d)[a]	B3LYP-PCM/ 6-31G(d)[a]	B3LYP/ 6-31G(d)[b]	B3LYP/ 6-31G(d)[c]
1	1.341	1.3741	1.3737	1.3701	1.3700
2	1.405	1.4192	1.4175	1.4209	1.4209
3	1.406	1.4192	1.4175	1.4219	1.4219
4	1.369	1.3663	1.3661	1.3517	1.3505
5	1.366	1.3663	1.3661	1.3510	1.3495
6	1.377	1.3893	1.3876	1.3850	1.3847
7	1.373	1.3893	1.3876	1.3850	1.3845
distance				6.3579[d]	6.0395[e]

[a] TOPDC. [b] Perchlorate TOPDC. [c] Hydrogen sulfate TOPDC. [d] The distance between two ClO_4^- ions. [e] The distance between two HSO_4^- ions.

Figure 2 shows the optimized geometry for the perchlorate TOPDC molecule. Two ClO_4^- ions lie above and under the TOPDC plane, respectively, with a Cl...Cl distance of ~6.4 Å. The counterions ClO_4^- hardly disturb the geometry of the TOPDC plane. Thus the local D_{4h} symmetry of the TOPDC plane is well preserved as is the case in the perchlorate TOPDC crystal. In general, the optimized structure is very close to that of the bare TOPDC. The maximum difference (0.015 Å) occurs at the type 5 C−O bond. The optimized geometry with ClO_4^-

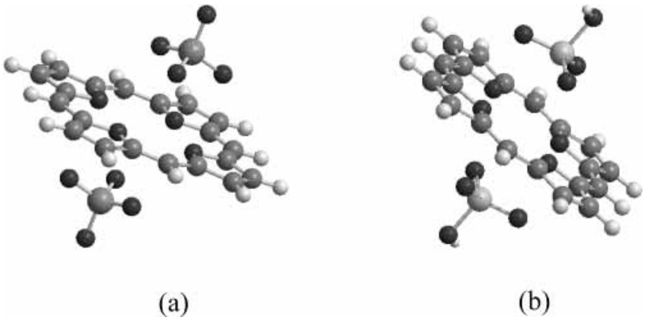

Figure 2. The optimized structures for the perchlorate tetraoxaporphyrin and hydrogen sulfate tetraoxaporphyrin.

counterions does show a slightly improved agreement with the crystallographically determined structure.

To see how the solvation will affect the geometry, we also performed the geometry optimization of TOPDC using the PCM. As shown by the data in Table 1, solvation only slightly compacted the molecule. The overall solvation effect on the geometry is negligible. The largest effect (0.0017 Å) takes place in the types 2 and 3 and types 6 and 7 C−C bonds.

Experimentally, it was found that perchlorate TOPDC is virtually insoluble in common organic solvent, while good solubility was achieved in concentrated sulfuric acid; thus the UV/vis spectra of TOPDC were obtained in 96% H_2SO_4 solution.[4] We calculated the reaction free energy change in solution as

$$\mathrm{TOPDC{-}(ClO_4)_2} + 2\mathrm{H_2SO_4} \rightarrow \mathrm{TOPDC^{2+}} + 2\mathrm{HSO_4^-} + 2\mathrm{HClO_4}$$

$$\Delta G(\mathrm{sol},\ 298\ \mathrm{K}) = -6.6\ \mathrm{kcal/mol}$$

$$\mathrm{TOPDC{-}(ClO_4)_2} \rightarrow \mathrm{TOPDC^{2+}} + 2\mathrm{ClO_4^-}$$

$$\Delta G(\mathrm{sol},\ 298\ \mathrm{K}) = -26.1\ \mathrm{kcal/mol}$$

Thus our calculations show that perchlorate TOPDC is indeed soluble in sulfuric acid, in agreement with the experimental observation.[4]

In Figure 2, we also depict the optimized geometry of the hydrogen sulfate TOPDC in the gas phase. Not surprisingly, we again find that the HSO_4^- counterions only interact with TOPDC electrostatically. Two HSO_4^- ions lie above and under the TOPDC plane, respectively, with a S...S distance of ∼6.0 Å. And we infer that the S...S distance will be further expanded when the effects of solvent of high dielectric constant and the hydrogen network of solvent molecules are explicitly taken into account. As seen in Figure 2, the local D_{4h} symmetry of the TOPDC plane is well preserved, and the optimized structure is very similar to that of the bare TOPDC such that bond distances differ by 0.0010 Å for types 2 and 3 and types 4 and 5 and by 0.0002 Å for types 6 and 7 (see Table 1). Thus we conclude that the geometry of TOPDC in solution is close to that in the crystal and the TOPDC bare ion plus the PCM for the solvation effect provides a reasonably good model for TOPDC in solution.

TABLE 2: Experimental and Optimized Bond Lengths (Å) for Porphycene under C_{2h} Symmetry

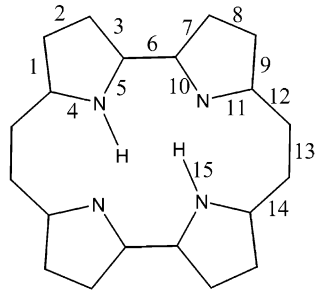

bond	X-ray (ref 23)	B3LYP/ 6-31G(d)(gas)	B3LYP-PCM/ 6-31G(d)(2-MTHF)
1	1.432	1.4349	1.4353
2	1.346	1.3778	1.3784
3	1.431	1.4311	1.4316
4	1.364	1.3673	1.3680
5	1.354	1.3638	1.3645
6	1.397	1.4128	1.4131
7	1.429	1.4497	1.4496
8	1.349	1.3651	1.3660
9	1.439	1.4559	1.4559
10	1.356	1.3529	1.3543
11	1.359	1.3613	1.3625
12	1.399	1.4127	1.4132
13	1.387	1.3942	1.3950
14	1.398	1.4079	1.4080
15		1.0425	1.0419

TABLE 3: Orbital Energies and Orbital Characters of TOPDC under D_{4h} Symmetry at the B3LYP/aug-cc-pVDZ Level

		orbital energy (au)	symmetry	orbital character
occupied MOs	76	−0.3640	A_{2u}	π
	77	−0.3548	B_{2u}	π
	78	−0.3513	E_g	π
	79	−0.3513	E_g	π
	80	−0.2853	A_{1u}	π
	81	−0.2845	A_{2u}	π
unoccupied MOs	82	−0.1744	E_g	π
	83	−0.1744	E_g	π
	84	−0.0987	B_{1u}	π
	85	−0.0697	B_{2u}	π
	86	−0.0186	E_g	π
	87	−0.0186	E_g	π
	88	0.0103	A_{1u}	π

The key X-ray data for porphycene are summarized in Table 2. The experimental structure possesses a near D_{2h} symmetry.[23,42] Experimentally it was found that the inner hydrogen atoms are not localized.[23] This shows that the crystallographically determined structure is at least the average of the two tautomeric trans-structures or even includes some contributions from the cis-structure.[23,42] Based on the experimental information as well as the previous theoretical results, we performed the geometry optimization on the *trans*-porphycene, which was concluded as the globe minimium.[23] Even though no symmetry constraint was imposed on the initial structure, the optimization converged to a structure of C_{2h} symmetry. The optimized geometry coincides with the classic [18]annulene model where the main conjugation path excludes the nitrogen atoms in the two pyrrol rings and the outer bonds in the two rings with the pyridine-like nitrogens.[41,43] Thus the type 2 C−C bond length differs from the type 8 C−C bond length by 0.0127 Å. In general, the optimized geometry of porphycene is in reasonable agreement with the experimental geometry,[23,42] although there is a tendency to overestimate the bond lengths. The average error for the 14 bond lengths is around 0.011 Å with a maximum of 0.032 Å occurring for the type 2 C−C bond. We have also optimized the geometry of porphycene in the 2-MTHF solvent. As porphycene is a neutral molecule and 2-MTHF is a solvent of low dielectric constant ($\epsilon = 6.97^{36}$), it is not surprising to see from Table 2 that the solvent has hardly any effect on the geometry of the porphycene solute. As compared to the gas-phase geometry, the mean deviation is only 0.0006 Å with the maximum deviation of 0.0013 Å occurring for the type 10 C−N bond.

TABLE 4: Orbital Energies and Characters of Porphycene with C_{2h} Symmetry at the B3LYP/aug-cc-pVDZ Level

		orbital energy (au)	symmetry	orbital character
occupied MOs	71	−0.3248	A_u	π
	72	−0.2918	B_g	π
	73	−0.2763	B_u	σ
	74	−0.2729	A_g	σ
	75	−0.2702	B_g	π
	76	−0.2627	A_u	π
	77	−0.2598	B_g	π
	78	−0.2405	A_u	π
	79	−0.2392	B_g	π
	80	−0.1963	A_u	π
	81	−0.1945	A_u	π
unoccupied MOs	82	−0.1045	B_g	π
	83	−0.0562	B_g	π
	84	−0.0092	A_u	π
	85	0.0146	A_u	Rydberg
	86	0.0372	B_g	π
	87	0.0762	A_u	Rydberg
	88	0.085	B_g	Rydberg
	89	0.0937	A_g	Rydberg

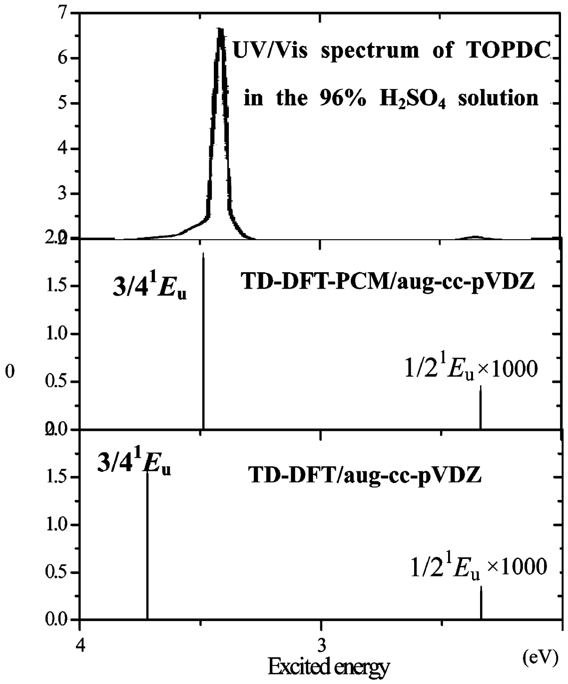

Figure 3. Experimental and calculated electronic excitation spectra for TOPDC (D_{4h}).

The frontier orbital energies and the corresponding orbital characters for the ground-state TOPDC are listed in Table 3. A few key orbitals around the HOMOs (highest occupied molecular orbitals) and LUMOs (lowest unoccupied molecular orbitals) are also presented in Table 3. Key frontier orbitals of the ground-state porphycene under C_{2h} symmetry are summarized in Table 4.

B. Singlet Vertical Excited States for TOPDC. The UV/vis spectrum of TOPDC in solution[4,5] is shown in the top panel of Figure 3, in which we observe the typical porphyrinoid type of spectrum with a weak band (Q band) in the low-energy region (2.34 eV) and a strong band (B band or Soret band) at around 3.35 eV.

To investigate the basis set effects on the excitation calculations, the singlet vertical excitation energies of TOPDC have been calculated at various levels. The TDDFT/6-31G(d), TDDFT/6-311G(d), and TDDFT/aug-cc-pVDZ results are shown in Table 5. As is well-documented, TDDFT results do not depend so much on the size of basis sets for the prediction of low-lying states. From Table 5, we see that these three basis sets virtually give identical results with differences of less than 0.06 eV. In the present study, the aug-cc-pVDZ basis set was adopted. With this basis set for TOPDC, the total number of basis functions is 512. The active space of TDDFT calculation consists of the complete molecular orbital space (488 MOs) except that the innermost 1s core orbitals for C and O atoms (24 MOs) were frozen.

As shown by Table 5, the lowest excitation energy part of the TOPDC spectrum consists of four $\pi-\pi^*$ excitations, two degenerate excitations (2.34 eV, $f = 0.0003$) for Q bands, and two degenerate excitations (3.72 eV, $f = 1.536$) for B (Soret) bands. This is similar to that of the free base porphin (FBP).[35] Gouterman explained the excitations of FBP according to his four-orbital model.[35] The four orbitals are HOMOs, h_1 and h_2, and LUMOs, l_1 and l_2. In his model, the four bands, Q_x, Q_y, B_x, and B_y, involve a "plus" or "minus"

TABLE 5: Main Configurations, Excitation Energies (*E*), and Oscillator Strengths (*f*) of TOPDC (D_{4h}) Calculated at Various Levels in the Gas Phase

	TDDFT(B3LYP)/6-31G(d)			TDDFT(B3LYP)/6-311G(d)			TDDFT(B3LYP)/aug-cc-pVDZ		
state	main configurations	*E* (eV)	*f*	main configurations	*E* (eV)	*f*	main configurations	*E* (eV)	*f*
1^1E_U	−0.43(80−82)+0.27(80−83) −0.27(81−82)−0.43 (81−83)	2.36	0.0006	0.42(80−82)−0.30(80−83) −0.299(81−82)−0.42(81−83)	2.34	0.0006	−0.49(80−82)+0.15(80−83) 0.16(81−82)+0.49(81−83)	2.34	0.0003
2^1E_U	0.27(80−82)+0.43(80−83) −0.43(81−82)+0.27(81−83)	2.36	0.0006	0.30(80−82)+0.42(80−83) 0.42(81−82)−0.30(81−83)	2.34	0.0006	0.15(80−82)+0.49(80−83) 0.49(81−82)−0.16(81−83)	2.34	0.0003
3^1E_U	−0.37(80−82)+0.37(81−83)	3.78	1.555	0.38(80−82)+0.38(81−83)	3.75	1.561	0.37(80−82)+0.36(81−83)	3.72	1.536
4^1E_U	0.37(80−83)+0.37(81−82)	3.78	1.555	−0.38(80−83)+0.38(81−82)	3.75	1.561	0.37(80−83)−0.36(81−82)	3.72	1.536
5^1E_U	0.11(76−82)−0.14(76−83) 0.40(77−82)+0.53(77−83)	4.30	0.032	−0.17(76−83)+0.66(77−83)	4.29	0.029	0.16(76−82)+0.11(77−82) 0.66(77−83)	4.29	0.027
6^1E_U	0.14(76−82)+0.11(76−83) 0.53(77−82)−0.40(77−83)	4.30	0.032	0.17(76−82)+0.66(77−82)	4.29	0.029	0.16(76−83)+0.66(77−82) −0.11(77−83)	4.29	0.027
7^1E_U	−0.19(76−82)+0.63(76−83) 0.17(77−83)	4.59	0.0004	0.28(76−82)+0.60(76−83) 0.15 (77−83)	4.57	0.0002	0.35(76−82)+0.57(76−83) −0.14 (77−82)	4.58	0.0001
8^1E_U	0.63(76−82)−0.19(76−83) −0.17(77−82)	4.59	0.0004	0.60(76−82)−0.28(76−83) −0.15 (77−82)	4.57	0.0002	0.57(76−82)−0.35(76−83) −0.14(77−83)	4.58	0.0001
9^1E_U	0.16(73−82)+0.64 (73 −83) 0.11 (81−87)	5.84	0.0002	0.66(73−83)+0.11(81−86)	5.81	0.0002	0.16(73−82)+0.64(73−83) 0.11(80−86)	5.80	0.0001
10^1E_U	0.65(73−82)−0.16(73−83) 0.11(81−86)	5.84	0.0002	0.66 (73−82)+0.11(81−87)	5.81	0.0002	0.65(73−82)−0.16(73−83) 0.11(80−87)	5.80	0.0001
11^1E_U	0.62(78−84)−0.17(79−84) −0.25(81−87)	6.33	0.015	0.54(78−84)+0.33(79−84) 0.23(81−86)+0.14(81−87)	6.32	0.016	0.59(78−84)−0.16(79−84) 0.31(80−86)	6.31	0.017
12^1E_U	0.17(78−84)+0.62(79−84) −0.25(81−86)	6.33	0.015	−0.33(78−84)+0.54(79−84) −0.14(81−86)+0.23(81−87)	6.32	0.016	0.16(78−84)+0.59(79−84) −0.31(80−87)	6.31	0.017

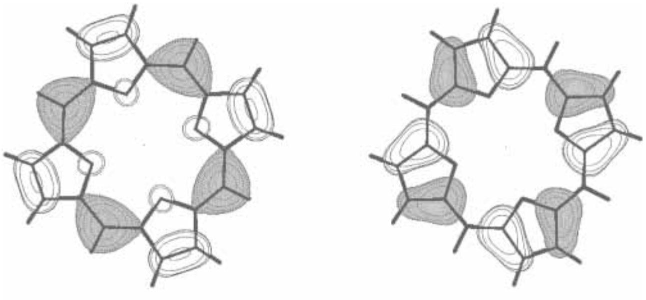

HOMO-1 (80) **HOMO (81)**

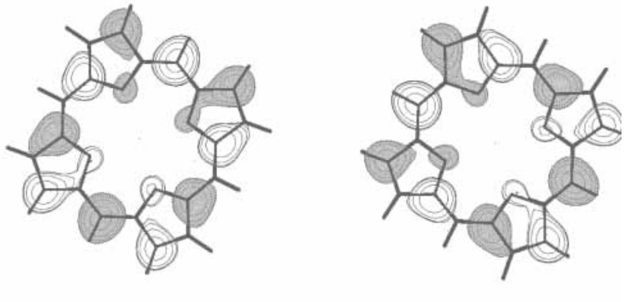

LUMO (82) **LUMO+1 (83)**

Figure 4. Contour maps of the occupied MOs (80, 81) and the unoccupied MOs (82, 83) for TOPDC.

combination of four single excitation configurations of similar weight:

$$\mathrm{Q}_x = (h_1 \rightarrow l_2) + (h_2 \rightarrow l_1)$$
$$\mathrm{Q}_y = (h_1 \rightarrow l_1) + (h_2 \rightarrow l_2)$$
$$\mathrm{B}_x = (h_1 \rightarrow l_2) - (h_2 \rightarrow l_1)$$
$$\mathrm{B}_y = (h_1 \rightarrow l_1) - (h_2 \rightarrow l_2)$$

We found that Gouterman's four-orbital model works well for the Q and B bands of TOPDC. Table 3 lists the frontier orbital energies and the corresponding orbital characters for the ground-state TOPDC. Thus MO 80 is h_1, MO 81 is h_2, MO 82 is l_1, and MO 83 is l_2. Contour maps of these four MOs are illustrated in Figure 4. As is expected from Gouterman's four-orbital model, LUMOs 82 and 83 are degenerate orbitals of e_g symmetry, while HOMOs 80 (a_{1u}) and 81 (a_{2u}) are quasi-degenerate with an energy difference of only 0.02 eV.

TDDFT calculations for TOPDC in the gas phase have captured the essence of the experimental UV−vis spectrum in solution, that is, a weak Q band accompanied by a strong B band. Even though the calculated Q band position (2.34 eV) is in remarkable agreement with the experimental excitation energies (2.34 eV[4,5,23]), the calculated B band position (3.72 eV) is 0.37 eV higher than the experimental excitation energies (3.35 eV[4,5,23]). This indicates that the solvent effect has to be taken into consideration.

The PCM has been successfully applied to describe the solvation effect on both the ground states and the excited states.[28−30] Specifically, it was found that the concentrated sulfuric acid solvent can be described satisfactorily by the continuum model in the applications of theoretical exploration of the reaction mechanisms of homogeneous catalysis.[47−49] For the TOPDC system, we find that the perchlorate ion will dissolve into the solution and that the solvent molecules HSO_4^- mainly interact with TOPDC electrostatically. As experiments showed that there is no excitation transfer from solute to solvent,[4,5,23,42] we expect that TDDFT combined with PCM provides a powerful tool to elucidate the UV−vis spectrum in solution. In the Gaussian 03 implementation,[28,40] we notice that electrostatic interaction described with static dielectric constant (ϵ) and fast dielectric constant (ϵ_f) makes a contribution to the solvent shifts of the excitation energies, while dispersion−repulsion contributions are included in the cavity terms described by numeral density (ρ) and solvent radius (R_{solv}) which do not contribute to the solvent shifts.

Table 6 summarizes the TDDFT-PCM results on the TOPDC (D_{4h}) system in solution. The results differ only marginally whether the gas-phase optimized geometry is employed or the solution-phase optimized geometry is used. We see that the predicted Q band (degenerate) is at 2.34 eV, in good agreement

TABLE 6: Main Configurations, Excitation Energies (*E*), and Oscillator Strengths (*f*) of TOPDC (D_{4h}) Calculated in the 96% H_2SO_4 Solution, Together with the Experimental Data of Excitation Energies (*E*) and the Corresponding Molar Extinction Coefficients

	TDDFT-PCM(B3LYP)/ aug-cc-pVDZ//B3LYP/6-31G(d)			TDDFT-PCM(B3LYP)/ aug-cc-pVDZ//B3LYP-PCM/6-31G(d)			experiment (refs 4 and 5)	
state	main configurations	*E* (eV)	*f*	main configurations	*E* (eV)	*f*	*E* (eV)	ϵ
1^1E_U	0.52(80−82)+0.51(81−83)	2.33	0.0004	0.40(80−82)−0.33(80−83) −0.33(81−82)−0.39(81−83)	2.34	0.0004	2.34−2.37 (Q)	1.86×10^4
2^1E_U	0.52(80−83)−0.51(81−82)	2.33	0.0004	0.33(80−82)+0.397(80−83) 0.39(81−82)−0.33(81−83)	2.34	0.0004		
3^1E_U	−0.39(80−82)+0.39(81−83)	3.48	1.785	0.30(80−82)−0.25(80−83) 0.25(81−82)+0.30(81−83)	3.49	1.79	3.35−3.53 (B)	1.02×10^6
4^1E_U	0.39(80−83)+0.39(81−82)	3.48	1.785	−0.25(80−82)−0.299(80−83) 0.30(81−82)−0.25(81−83)	3.49	1.79		
5^1E_U	−0.15(76−83)+0.23(77−82) 0.63(77−83)	4.31	0.015	0.11(76−82)+0.12(76−83) −0.45(77−82)+0.49(77−83)	4.32	0.015		
6^1E_U	0.15(76−82)+0.63(77−82) −0.23(77−83)	4.31	0.015	−0.12(76−82)+0.11(76−83) 0.49(77−82)+0.45(77−83)	4.32	0.015		
7^1E_U	0.67(76−83)+0.16(77−83)	4.60	0.001	0.48(76−82)−0.46(76−83) 0.11(77−82)+0.11(77−83)	4.61	0.001		
8^1E_U	0.67(76−82)−0.16(77−82)	4.60	0.001	0.46(76−82) 0.48(76−83) 0.11(77−82)−0.11(77−83)	4.61	0.001		
9^1E_U	−0.45(73−82)+0.50(73−83)	5.78	0.0001	−0.43(73−82)+0.51(73−83)	5.79	0.0001		
10^1E_U	0.50(73−82)+0.45(73−83)	5.78	0.0001	0.51(73−82)+0.43(73−83)	5.79	0.0001		
11^1E_U	0.56(78−84)−0.11(79−85) −0.14(80−87)−0.38(81−88)	6.31	0.0200	−0.43(78−84)+0.36(79−84) 0.29(80−87)+0.11(81−88)+0.24(81−88)	6.32	0.0200		
12^1E_U	0.11(78−85)+0.56(79−84) 0.14(80−88)−0.38(81−87)	6.31	0.0200	−0.36(78−84)+0.43(79−84) 0.11(80−88)−0.29(81−87)+0.24(81−88)	6.32	0.0200		

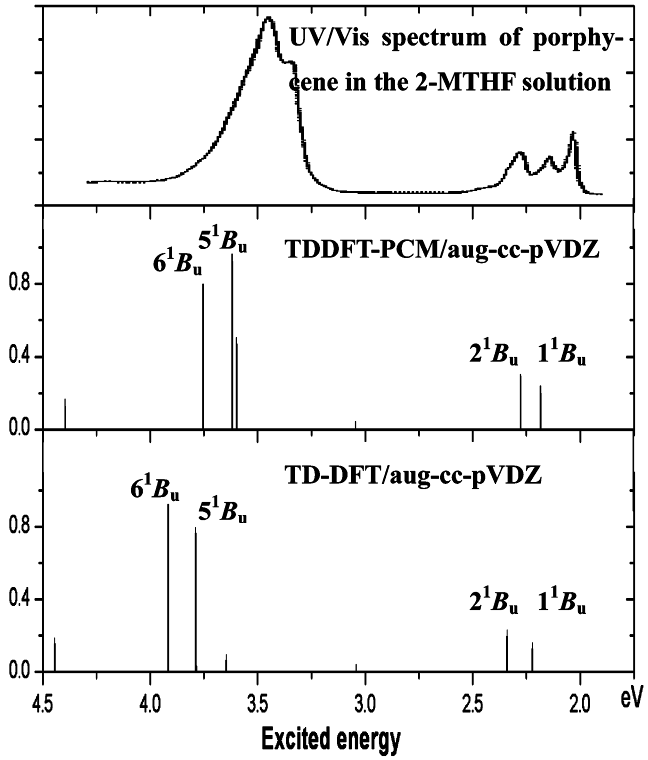

Figure 5. Experimental and calculated electronic excitation spectra for porphycene (C_{2h}).

with the experimentally measured value (2.34 eV). The corresponding calculated oscillator strengths are around 0.0004, which are consistent with the experimentally observed very weak peak.

Our calculated excitation energies for the B band are now 3.49 eV (degenerate). The solvation effects result in a 0.23 eV red shift for the Soret states, which brings the theoretical number much closer to the experimentally measured value of 3.35 eV.[4,5,23] We find that the calculated oscillator strengths for the B band are 1.536 in the gas phase and 1.786 in solution, which are consistent with the experimentally observed very strong peak of the B band.[4,5,23] In the higher energy region, we also predict a couple of valence $\pi-\pi^*$ singlet excited states with small oscillator strengths (see Table 6 for details). Specifically, we tentatively assign the peak at 4.32 eV ($f = 0.015$) to the weak shoulder at the high-energy side of the B band of TOPDC in solution (see Figure 3).

It is interesting to notice that solvation effects do not shift the Q band but significantly red-shift the B band. As spectral shift is largely influenced by the dipole change in going from the ground state to the excited states, we conclude that there is little change of dipole moment from the ground state to Q band states, while substantial dipole change occurs from the ground state to B band states. We notice that there is still a discrepancy of 0.14 eV between theory and experiment for the B band. The inherent limitation of the PCM may be responsible for this disagreement.

To our knowledge, no previous ab initio study is available for the absorption spectrum of TOPDC, although there were several theoretical studies at the semiempirical levels.[23] The most recent one was based on INDO/S calculations of TOPDC (D_{4h}) in vacuo.[23] The results are less satisfactory, leading to the Q band at 2.17 eV and the B band at 4.40 eV.[23]

C. Singlet Vertical Excited States for Porphycene. The experimental absorption spectrum of porphycene in the 2-MTHF solution,[23,42] together with the TDDFT theoretical spectra both

TABLE 7: Main Configurations, Excitation Energies (*E*), and Oscillator Strengths (*f*) of Porphycene (C_{2h}) Calculated in the Gas Phase and the 2-MTHF Solution, Together with the Experimental Data

	TDDFT(B3LYP)/ aug-cc-pVDZ//B3LYP/6-31G(d)			TDDFT-PCM(B3LYP)/ aug-cc-pVDZ//B3LYP/6-31G(d)			TDDFT-PCM(B3LYP)/ aug-cc-pVDZ//B3LYP-PCM/6-31G(d)			experiment (ref 43)	
state	main configurations	*E* (eV)	*f*	main configurations	*E* (eV)	*f*	main configurations	*E* (eV)	*f*	*E* (eV)	*f*
1^1B_u	0.12(78−82)+0.55(80−82) −0.21(81−82)−0.32(81−83)	2.22	0.13	0.10(78−82)+0.57(80−82) −0.21(81−82)−0.29(81−83)	2.19	0.20	0.10(78−82)+0.57(80−82) −0.21(81−82)−0.29(81−83)	2.19	0.20		
2^1B_u	0.19(80−82)+0.30(80−83) 0.54(81−82)−0.14(81−83)	2.33	0.20	0.20(80−82)+0.27(80−83) 0.56(81−82)−0.13(81−83)	2.28	0.30	0.20(80−82)+0.27(80−83) 0.56(81−82)−0.13(81−83)	2.28	0.30	1.94−2.17 (Q)	0.12
3^1B_u	0.66(78−82)+0.20(81−83)	3.04	0.003	0.66(78−82)+0.19(81−83)	3.05	0.004	0.66(78−82)+0.19(81−83)	3.04	0.004		
4^1B_u	0.61(76−82)+0.20(80−83) −0.20(81−83)	3.64	0.11	0.48(76−82)−0.10(80−82) 0.21(80−83)−0.36(81−83)	3.60	0.47	0.48(76−82)−0.10(80−82) 0.23(80−83)−0.36(81−83)	3.60	0.47		
5^1B_u	−0.12(78−82)+0.45(80−83) −0.12(81−82)+0.33(81−83)	3.75	0.80	−0.11(78−82)+0.50(80−83) −0.11(81−82)+0.31(81−83)	3.62	0.91	−0.11(78−82)+0.49(80−83) −0.11(81−82)+0.32(81−83)	3.62	0.93	3.26−3.41 (B)	1.32
1^1A_u	0.70(73−82)	3.78	0.00	0.70(73−82)	3.81	0.0000	0.70(73−82)	3.81	0.0000		
6^1B_u	0.32(76−82)+0.14(80−82) −0.29(80−83)+0.37(81−83)	3.87	0.92	0.49(76−82)+0.11(80−82) −0.26(80−83)+0.29(81−83)	3.76	0.84	0.49(76−82)+0.11(80−82) −0.25(80−83)+0.29(81−83)	3.76	0.83		
7^1B_u	0.68(78−83)	4.41	0.15	0.69(78−83)	4.41	0.12	0.69(78−83)	4.40	0.13		
2^1A_u	0.70(81−86)	4.96	0.001	0.69(73−83)	5.01	0.0006	0.69(73−83)	4.99	0.0006		
8^1B_u	0.67(76−83)+0.16(80−90)	4.99	0.02	0.68(76−83)+0.15(80−89)	4.98	0.03	0.68(76−83)+0.15(80−89)	4.98	0.03		
3^1A_u	0.68(73−83)−0.11(80−86)	4.98	0.000	0.70(81−86)	5.04	0.0006	0.70(81−86)	5.04	0.0006		
4^1A_u	0.11(73−83)+0.69(80−86)	5.02	0.003	0.70(80−86)	5.09	0.004	0.70(80−86)	5.09	0.004		
9^1B_u	0.24(71−82)+0.64 (81−90)	5.36	0.10	0.25(71−82)+0.64(81−89)	5.38	0.11	0.26(71−82)+0.64(81−89)	5.38	0.11		

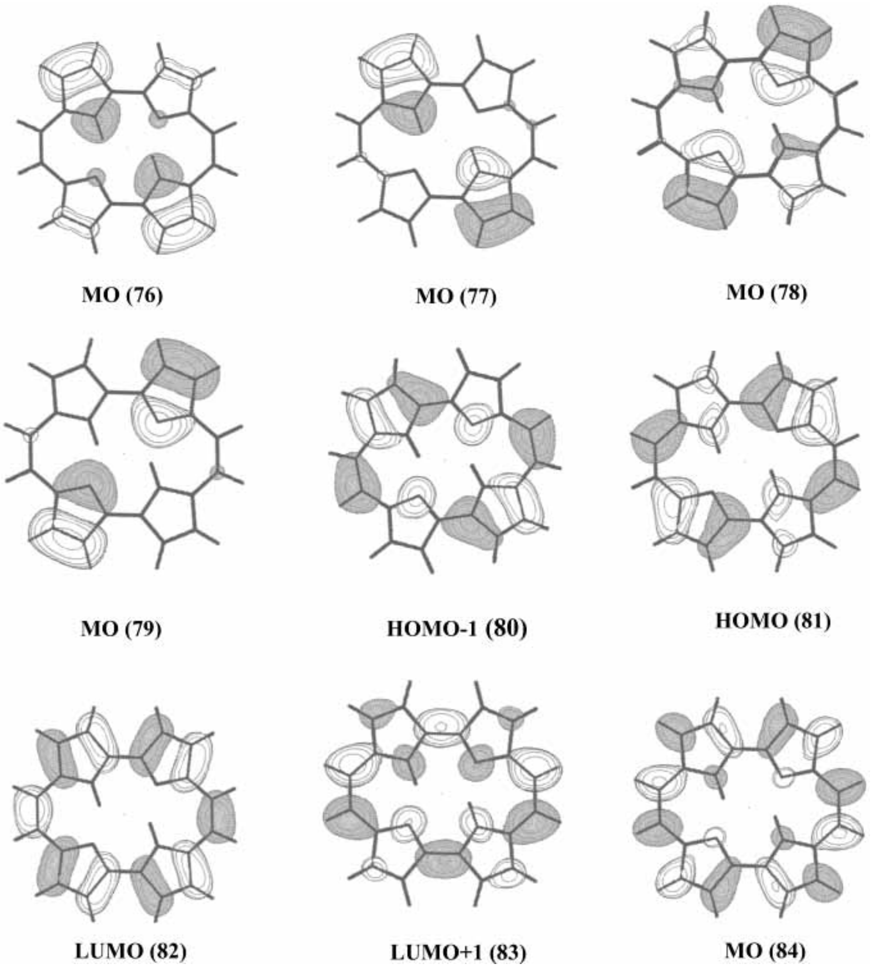

Figure 6. Contour maps of the occupied MOs (76, 77, 78, 79, 80, 81) and the unoccupied MOs (82, 83, 84) for porphycene.

in vacuo and in 2-MTHF solution, is illustrated in Figure 5. The theoretical details are summarized in Table 7. For TDDFT-PCM calculations, the geometries optimized both in vacuo and in solution were used. For porphycene with the aug-cc-pVDZ basis set, the total number of basis functions is 522. The active space of TDDFT calculation consists of the complete molecular orbital space (498 MOs) with the exception of the innermost 1s core orbitals for C and N atoms such that 24 MOs were frozen.

As is shown by the main configurations listed in Table 7, we find that, as compared to the cases of TOPDC and FBP, Gouterman's four-orbital model works less well for the Q band and breaks down for the description of the B band of porphycene. Table 4 summarizes some key orbitals of the ground-state porphycene under C_{2h} symmetry. The contour maps of some key orbitals are depicted in Figure 6. Here again MOs 80 and 81 are the HOMOs, while MOs 82 and 83 are the LUMOs. HOMOs can still be considered as degenerate, with a variation of 0.049 eV for the orbital energies of MOs 80 and 81. LUMOs, however, are no longer degenerate. The splitting between MO 82 and MO 83 is as large as 1.31 eV.

As shown in Table 7, we assign the first two states 1^1B_u and 2^1B_u to the Q_x and Q_y excitations, which involve mainly the excitations between HOMOs and LUMOs. Noteworthily, the (78 → 82) excitation also makes a non-negligible contribution. For the B band of porphycene, however, besides the excitations from HOMOs to LUMOs, (76 → 82) and (78 → 82) excitations also play an important role. Inspection of the orbital energies of porphycene in Table 4 shows that the energy gap between MO 76 and MO 82 is 4.30 eV, while that between MO 78 and MO 82 is only 3.70 eV. On the contrary, data in Table 3 for TOPDC indicate that the energy gap between MO 76 and MO 82 is 5.16 eV, while that between MO 78 and MO 82 is 4.81 eV, much larger than the corresponding values of porphycene. Thus we conclude that the decreased energy gap between the inner key orbitals and the frontier orbitals accounts for the inadequacy of the four-orbital model.

We calculated 1^1B_u and 2^1B_u states at 2.22 and 2.33 eV in the gas phase and 2.19 and 2.28 eV in the 2-MTHF solution. These numbers are close to the experimentally measured values of 1.94 (Q_x) and 2.17 (Q_y) eV. The corresponding calculated oscillator strengths are 0.127 and 0.197 in vacuo and 0.198 and 0.296 in solution, which are consistent with the experimental observation that the Q band of porphycene is much stronger than that of TOPDC or FBP. In the experimental spectrum (Figure 5), there is a third peak at 2.24 eV, which is absent in the present TDDFT calculations. As this peak also appears in the substituted free bases and moves with the onset of Q_y, it is therefore a vibrational band of Q_y.

We calculated the 4^1B_u state at 3.64 eV with an oscillator strength of 0.106 in the gas phase and 3.60 eV with an oscillator strength of 0.468 in 2-MTHF solution. From Table 7, we find that the coefficients of the main configurations change upon solvation from 0.61*(76 → 82) − 0.20*(81 → 83) in the gas phase to 0.48*(76 → 82) − 0.36*(81 → 83) in the solution phase. The increased coefficient of valence configuration (81 → 83) is most likely responsible for the enhanced oscillator strength in solution.

We predicted the 5^1B_u state at 3.75 eV with an oscillator strength of 0.797 in the gas phase and 3.62 eV with an oscillator strength of 0.927 in the 2-MTHF solution. We also found that the 6^1B_u state was at 3.87 eV ($f = 0.920$) in vacuo and 3.76 eV ($f = 0.828$) in solution. Based on the main configurations, excitation energies, and oscillator strengths, we concluded that the 4^1B_u, 5^1B_u, and 6^1B_u states are responsible for the broad and strongest B band of porphycene. The solvation effects give rise to a red shift of around 0.13 eV for the Soret states of 5^1B_u and 6^1B_u, which leads to a closer agreement with the experimentally measured value of 3.26−3.41 eV. [23,42]

Experimentally,[23,42] there exists a very weak peak at 3.10 eV, which is between the Q band and the B band. This peak is unique for porphycene and is not seen in TOPDC. We located this peak at 3.04 eV with $f = 0.004$. Our calculations showed that this peak is mainly contributed from the (78 → 82) excitation, with some contribution from (81 → 83). As compared to the gas-phase spectrum, we found this peak does not shift upon solvation.

In the higher energy region, a couple of valence $\pi-\pi^*$ singlet excited states were calculated with smaller oscillator strengths (see Table 7 for details). Among others, we predicted the 7^1B_u state at 4.40 eV with an oscillator strength of 0.126 in the 2-MTHF solution.

To our knowledge, no previous ab initio study is available for the absorption spectrum of porphycene. An earlier semiempirical calculation of porphycene (C_{2h}) in vacuo using CNDO/S predicted 1.84 and 2.17 eV for the Q band and 3.98 and 4.33 eV for the B band.[23] These results are less satisfactory, with the B band being overestimated by ∼1 eV.

IV. Conclusions

We have investigated the vertical electronic excitations of tetraoxaporphyrin dication (TOPDC) and porphycene by using the TDDFT method. The solvation effects have been taken into account through the PCM. Our calculations show that while Gouterman's four-orbital model works well for the TOPDC system, it breaks down for the porphycene system. We attribute the inadequacy of the four-orbital model to the decrease in orbital gaps in the porphycene system. We find that there are red shifts of around 0.23 eV for the Soret states of TOPDC and about 0.13 eV for the Soret states of porphycene. TDDFT-PCM calculations lead to a closer agreement with the measured values of experimental absorption spectra in solutions, which demonstrates the importance of taking into account the solvation effects for interpreting experimental absorption spectra in solution.

Acknowledgment. The present study is supported by the China Scholarship Council, the National Natural Science Foundation of China (Nos. 20203009, 20021002, and 29973031), the Natural Science Foundation of Hubei Province (No. 2002AB056), the Ministry of Science and Technology of China (2001CB610506), and TRAPOYT from the Ministry of Education of China.

References and Notes

(1) Franck, B.; Nonn, A. *Angew. Chem.* **1995**, *107*, 1941.

(2) Vogel, E. *Pure Appl. Chem.* **1993**, *65*, 143.

(3) Vogel, E.; Kocher, M.; Schmickler, H.; Lex, J. *Angew. Chem.* **1986**, *98*, 262.

(4) Vogel, E.; Haas, W.; Knipp, B.; Lex, J.; Schmickler, H. *Angew. Chem.* **1988**, *100*, 445; 448. Vogel, E.; Haas, W.; Knipp, B.; Lex, J.; Schmickler, H. *Angew. Chem., Int. Ed. Engl.* **1988**, *27*, 406.

(5) Bachmann, R.; Cerson, F.; Cescheidt, C.; Vogel, E. *J. Am. Chem. Soc.* **1992**, *114*, 10855.

(6) Vogel, E. *J. Heterocycl. Chem.* **1996**, *33*, 1461.

(7) Furuta, H.; Asano, T.; Ogawa, T. *J. Am. Chem. Soc.* **1994**, *116*, 767.

(8) Chmielewski, P. J.; Latos-Grazynski, L.; Rachlewicz, K.; Glowiak, T. *Angew. Chem., Int. Ed. Engl.* **1994**, *33*, 779.

(9) Vogel, E.; Pohl, M.; Herrmann, A.; Wib, T.; Konig, C.; Lex, J.; Gross, M.; Gisselbrecht, J. P. *Angew. Chem.* **1996**, *108*, 1677.

(10) Furuta, H.; Morimoto, T.; Osuka, A. *Inorg. Chem.* **2004**, *43*, 1618.

(11) Furuta, H.; Maeda, H.; Osuka, A. *Chem Commun.* **2002**, 1795.

(12) Doughery, T. J. *Adv. Photochem.* **1992**, *17*, 275.

(13) Schick, G. A.; O'Grady, M. R.; Tiwari, R. K. *J. Phys. Chem.* **1993**, *97*, 1339.

(14) Pasternack, R. F.; Schaefer, K. F.; Hambright, P. *Inorg. Chem.* **1994**, *33*, 2062.

(15) Ribo, J. M.; Crusats, J.; Farrera, J. A.; Valero, M. L. *J. Chem. Soc., Chem. Commun.* **1994**, 681.

(16) Akins, D. L.; Ozcelik, S.; Zhu, H. K.; Guo, C. *J. Phys. Chem. A* **1997**, *101*, 3251.

(17) Akins, D. L.; Zhu, H. K.; Guo, C. *J. Phys. Chem.* **1996**, *100*, 14390.

(18) Akins, D. L.; Ozcelik, S.; Zhu, H. K.; Guo, C. *J. Phys. Chem.* **1996**, *100*, 5420.

(19) Tokita, Y.; Hasegawa, J.; Nakatsuji, H. *J. Phys. Chem. A* **1998**, *102*, 1843.

(20) Serrano-Andres, L.; Merchan, M.; Rubio, M.; Roos, B. O. *J. Chem. Phys.* **1999**, *108*, 4439.

(21) Gwaltney, S. R.; Bartlett, R. J. *J. Chem. Phys.* **1998**, *108*, 6790.

(22) van Gisbergen, S. J. A.; Rosa, A.; Ricciardi, G.; Baerends, E. J. *J. Chem. Phys*. **1999**, *111*, 2499.

(23) Malsch, K.; Roeb, M.; Karuth, V.; Hohlneicher, G. *Chem. Phys.* **1998**, *227*, 331.

(24) Chen, D. M.; He, T. J.; Cong, D. F.; Zhang, Y. H.; Liu, F. C. *J. Phys. Chem. A* **2001**, *105*, 3981.

(25) Bauernschmitt, R.; Ahlrichs, R. *Chem. Phys. Lett.* **1996**, *256*, 454.

(26) Casda, M. E.; Jamorski, C.; Casida, K. C.; Salahub, D. R. *J. Chem. Phys.* **1998**, *108*, 4439.

(27) Stratmann, R. E.; Scuseria, G. E.; Frisch, M. J. *J. Chem. Phys.* **1998**, *109*, 8218.

(28) Cossi, M.; Barone, V. *J. Chem. Phys.* **2001**, *115*, 4708.

(29) Miertus, S.; Scrocco, E.; Tomasi, J. *Chem. Phys.* **1981**, *55*, 117.

(30) Barone, V.; Cossi, M.; Tomasi, J. *J. Chem. Phys.* **1997**, *107*, 3210.

(31) Becke, A. D. *J. Chem. Phys.* **1993**, *98*, 5648.

(32) Becke, A. D. *Phys. Rev. A* **1988**, *38*, 3098.

(33) Slater, J. C. *Quantum Theory of Molecular and Solids. Vol. 4*: *The Self-Consistent Field for Molecular and Solids*; McGraw-Hill: New York, 1974.

(34) Vosko, S. H.; Wilk, L.; Nusair, M. *Can. J. Phys*. **1980**, *58*, 1200.

(35) Lee, C.; Yang, W.; Parr, R. G. *Phys. Rev. B* **1988**, *37*, 785.

(36) Physical Properties. In *Lange's Handbook of Chemistry*, 15th ed.; Dean, J. A., Ed.; McGraw-Hill: New York, 1999.

(37) Ditchfield, R.; Hehre, W. J.; Pople, J. A. *J. Chem. Phys.* **1971**, *54*, 724.

(38) Kendall, R. A.; Dunning, T. H., Jr.; Harrison, R. J. *J. Chem. Phys.* **1992**, *96*, 6796.

(39) Dunning, T. H., Jr. *J. Chem. Phys.* **1989**, *90*, 1007.

(40) Frisch, M. J.; Trucks, G. W.; Schlegel, H. B.; Scuseria, G. E.; Robb, M. A.; Cheeseman, J. R.; Montgomery, J. A., Jr.; Vreven, T.; Kudin, K. N.; Burant, J. C.; Millam, J. M.; Iyengar, S. S.; Tomasi, J.; Barone, V.; Mennucci, B.; Cossi, M.; Scalmani, G.; Rega, N.; Petersson, G. A.; Nakatsuji, H.; Hada, M.; Ehara, M.; Toyota, K.; Fukuda, R.; Hasegawa, J.; Ishida, M.; Nakajima, T.; Honda, Y.; Kitao, O.; Nakai, H.; Klene, M.; Li, X.; Knox, J. E.; Hratchian, H. P.; Cross, J. B.; Adamo, C.; Jaramillo, J.; Gomperts, R.; Stratmann, R. E.; Yazyev, O.; Austin, A. J.; Cammi, R.; Pomelli, C.; Ochterski, J. W.; Ayala, P. Y.; Morokuma, K.; Voth, G. A.; Salvador, P.; Dannenberg, J. J.; Zakrzewski, V. G.; Dapprich, S.; Daniels, A. D.; Strain, M. C.; Farkas, O.; Malick, D. K.; Rabuck, A. D.; Raghavachari, K.; Foresman, J. B.; Ortiz, J. V.; Cui, Q.; Baboul, A. G.; Clifford, S.; Cioslowski, J.; Stefanov, B. B.; Liu, G.; Liashenko, A.; Piskorz, P.; Komaromi, I.; Martin, R. L.; Fox, D. J.; Keith, T.; Al-Laham, M. A.; Peng, C. Y.; Nanayakkara, A.; Challacombe, M.; Gill, P. M. W.; Johnson, B.; Chen, W.; Wong, M. W.; Gonzalez, C.; Pople, J. A. *Gaussian 03*, revision B.03; Gaussian, Inc.: Pittsburgh, PA, 2003.

(41) Gouterman, M. *J. Chem. Phys.* **1959**, *30*, 1139.

(42) Dietrich, H. J. Ph.D. Thesis, Cologne, 1993.

(43) Waluk, J.; Muller, M.; Swiderek, P.; Kocher, M.; Vogel, E.; Hohlneicher, G.; Michl, J. *J. Am. Chem. Soc.* **1991**, *113*, 551.

(44) Baerends, E. J.; Ricciardi, G.; Rosa, A.; van Gisbergen, S. J. A. *Coord. Chem. Rev.* **2002**, *230*, 5.

(45) Hashimoto, T.; Choe, Y.-K.; Nakano, H.; Hirao, K. *J. Phys. Chem. A* **1999**, *103*, 1894.

(46) Nakatsuji, H.; Hasegawa, J.; Hada, M. *J. Chem. Phys.* **1996**, *104*, 2321.

(47) Mylvaganam, K.; Bacskay, G. B.; Hush, N. S. *J. Am. Chem. Soc*. **2000**, *122*, 2041.

(48) Gilbert, T. M.; Hristov, I.; Ziegler, T. *Organometallics* **2001**, *20*, 1183.

(49) Kua, J.; Xu, X.; Periana, R. A.; Goddard, W. A., III *Organometallics* **2002**, *21*, 511.